AIAA JOURNAL
Vol. 33, No. 12, December 1995

Modal Analysis Using Segmented Piezoelectric Sensors

J. Callahan* and H. Baruh†
Rutgers University, Piscataway, New Jersey 08855-0909

This paper is concerned with the use of segmented piezoelectric film sensors for the modal analysis of structures. We make use of the relation between the charge generated by the piezoelectric sensors and the modal coordinates, the asymptotic behavior of the eigensolution of structures, and the concept of modal observers to extract the modal coordinates and velocities from the sensor output. We also conduct sensitivity studies in an effort to determine the optimal coverage area of the piezofilm sensor, and we investigate the effects of noise, unmodeled dynamics, and parameter errors on the accuracy of the modal coordinate and velocity extraction. We analyze implementation of piezoelements on beams as well as on plates.

I. Introduction

In the past few years, the introduction of piezoelectric film components for motion sensing and control has changed the nature of vibration measurement and analysis tremendously. Hardware issues that have plagued experimentalists in the past, such as cost, size, weight, number, and reliability of sensors have almost disappeared with the introduction of piezofilm components. The potential that such components have is evident from the interest these materials have generated.[1-8]

Piezosensors in a sense can be treated as piecewise continuous or continuous sensors, with the exception that a single electrical signal comes out of each sensor. For beams, various sensor weightings have been proposed. In Ref. 9, segmented piezosensors are used to general displacement profiles. In that study, it is determined that for static deflection measurements, sensor shape has a strong effect on the sensor's ability to filter out higher modes. For dynamic beam response, modal sensors have been proposed[5] in which there are film elements running throughout the beam which are cut into shapes proportional to the second derivative of the eigenfunctions. By virtue of the orthogonality with respect to the stiffness of the structure, the piezosensor acts as an orthogonal filter, giving a charge signal directly proportional to the amplitude of the associated mode. The advantage of this approach is that it gives the modal coordinate directly, with no computational effort and excellent accuracy.[1,5] The disadvantage is that the procedure requires one layer of film which has to be cut into a prescribed shape and must span the entire length of the beam for each observed mode, making it difficult to extract several modal amplitudes. The approach becomes even more complicated for two-dimensional structures.

In this paper we analyze the application of segmented piezoelectric film sensors to modal analysis and, specifically, to the extraction of several modal coordinates and velocities from the system output. In addition to the approach by Lee and Moon,[5] the process of obtaining modal information from traditional sensors will be in the form of modal filters or full-order observers.[10,11] Using simple piezosensor geometries together with modal observers gives satisfactory results while still allowing for variations in structural mass and stiffness.

II. Sensor Equation

A linear piezoelectric plate theory that incorporates the piezoelectric effect into the classic laminate constitutive equations has been formulated by Lee.[12] For a thin laminate, the displacements of any point are characterized by the deformation of the geometric midplane. If the in-plane displacements u_0 and v_0 are assumed to be negligible compared to the transverse deflection w and the output signal is generated by deformation only, then the charge $q_r(t)$ generated by each piezoelectric lamina is approximated by

$$q_r(t) = -\bar{z}_r \int_0^a \int_0^b \{F(x,y)P_0(x,y)L_p[w(x,y,t)]\}_r \, dx\, dy \qquad (r = 1, 2, \ldots, N) \quad (1)$$

where

$$L_p = e_{31}^0 \frac{\partial^2}{\partial x^2} + e_{32}^0 \frac{\partial^2}{\partial y^2} + 2e_{36}^0 \frac{\partial^2}{\partial x \partial y} \qquad (2)$$

$$F_r(x,y) = \begin{cases} 1, & \text{if } (x,y) \text{ is within the } r\text{th sensor coverage} \\ 0, & \text{otherwise} \end{cases}$$

Here, e_{31}^0, e_{32}^0, and e_{36}^0 are piezoelectric [(charge/area)/strain] constants and $P_0(x,y)$ accounts for polarity variations in the material. For a rectangular plate, a, b, and h are the respective length, width, and height of the overall laminate. The quantity $\bar{z}_r$ is the distance from the geometric center of the rth sensor to the midplane of the laminate and N is the number of piezosensors. Figure 1 shows the coordinate axes and dimensions for a rectangular laminate with piezosensor coverage.

One-Dimensional Case: Composite Beam

If the midplane displacement has no y dependence, then Eq. (1) simplifies to the one-dimensional sensor equation

$$q_r(t) = -e_{31,r}^0 \bar{z}_r \int_0^a \mathcal{F}_r(x) \frac{\partial^2 w(x)}{\partial x^2} \, dx \qquad (3)$$

where

$$\mathcal{F}_r(x) = \int_{-\frac{b}{2}}^{\frac{b}{2}} F_r(x,y) P_{0,r}(x,y) \, dy$$

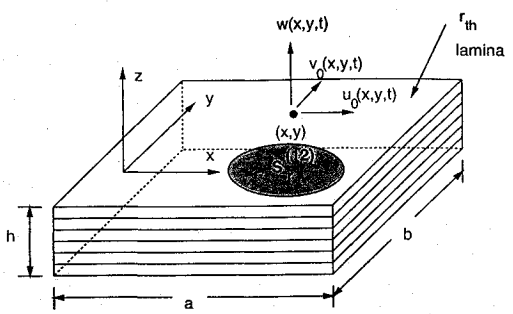

Fig. 1 Composite plate with surface electrode.

Received May 17, 1994; revision received Feb. 15, 1995; accepted for publication Feb. 15, 1995.

*Graduate Assistant, Department of Mechanical and Aerospace Engineering.
†Associate Professor, Department of Mechanical and Aerospace Engineering. Member AIAA.

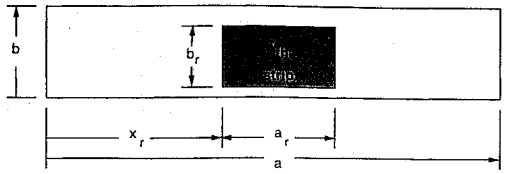

Fig. 2 Piezoelectric strip dimensions for a beam.

From linear vibration theory, the transverse displacement of the beam can be expressed as a linear combination of the natural modes given by

$$w(x,t) = \sum_{s=1}^{\infty} w_s(x)\eta_s(t) \tag{4}$$

where $w_s(x)$ and $\eta_s(t)$ are the mode shape and corresponding modal coordinate of the sth mode. After substitution of Eq. (4) into Eq. (3), the one-dimensional modal sensor equation can be expressed in vector form as

$$\{q(t)\} = [B]\{\eta(t)\} \tag{5}$$

where

$$B_{rs} = -e^0_{31,r}\bar{z}_r \int_0^a \mathcal{F}_r(x)\frac{\mathrm{d}^2 w_s(x)}{\mathrm{d}x^2}\,\mathrm{d}x \tag{6}$$

The entries of $[B]$ need to be calculated only when the eigensolution of the structure changes. Note that for an exact modal expansion, the matrix $[B]$ has dimension $N \times \infty$. The next step is to choose the variation of the spatial electrode pattern $\mathcal{F}_r(x)$ for each layer.

Lee and Moon[5] have shown that if the spatial electrode pattern of the rth lamina is of the form

$$\mathcal{F}_r(x) = \mu_r \frac{\mathrm{d}^2 w_r(x)}{\mathrm{d}x^2} \tag{7}$$

one obtains a true modal sensor based on the orthogonality of the eigensolution of the beams with respect to their stiffnesses. Here, the arguments μ_r are scaling constants. For this choice, the entries of $[B]$ are given by

$$B_{rs} = -\frac{\mu_r e^0_{31,r}\bar{z}_r\omega_r^2}{D_E}\delta_{rs} \tag{8}$$

where ω_r is the vibration frequency of the rth mode and D_E is the effective elastic bending modulus of the laminate. Since $[B]$ is diagonal, each mode can be sensed directly. Note, however, that the lamina must span the entire length of the beam (integral is from 0 to a). This can be done with relative ease for beams, since the laminae can be put side by side along the beam width or a few of them can be stacked, but the sensors must also be cut into specific patterns due to the requirement of $\mathcal{F}_r(x)$. This approach may not be feasible for structures with complicated geometries or whose mass and stiffness properties may change.

Rather than etch the lamina into complicated full-length patterns, one can place segmented strips at various locations on the beam. The spatial pattern of the rth strip in Fig. 2 has the form

$$\mathcal{F}_r(x) = b_r[H(x - x_r) - H(x - x_r - a_r)] \tag{9}$$

where x_r is the left-hand x coordinate of the rth strip, a_r is its length, b_r is its width (not necessarily the width of the beam), and $H(x)$ is the spatial Heaviside step function. Putting Eq. (9) into Eq. (6) yields

$$B_{rs} = -e^0_{31,r}\bar{z}_r b_r\left[\left.\frac{\mathrm{d}w_s(x)}{\mathrm{d}x}\right|_{x_r+a_r} - \left.\frac{\mathrm{d}w_s(x)}{\mathrm{d}x}\right|_{x_r}\right] \tag{10}$$

Note that the $[B]$ matrix is now fully populated.

Two-Dimensional Case I: Rectangular Composite Plate

We consider here plates subjected to boundary conditions which permit orthogonalization. A simply supported rectangular plate is one such case. From linear vibration theory for plates, the plate deflection can be decomposed into its constituent modes using

$$w(x,y,t) = \sum_{l=1}^{\infty}\sum_{m=1}^{\infty} w_{lm}(x,y)\eta_{lm}(t) \tag{11}$$

Substituting Eq. (11) into Eq. (1) and arranging the modal coordinates according to

$$\begin{bmatrix} \eta_1 & \eta_2 & \eta_5 & \cdots \\ \eta_3 & \eta_4 & \eta_7 & \cdots \\ \eta_6 & \eta_8 & \eta_9 & \cdots \\ \vdots & \vdots & \vdots & \ddots \end{bmatrix} = \begin{bmatrix} \eta_{11} & \eta_{12} & \eta_{13} & \cdots \\ \eta_{21} & \eta_{22} & \eta_{23} & \cdots \\ \eta_{31} & \eta_{32} & \eta_{33} & \cdots \\ \vdots & \vdots & \vdots & \ddots \end{bmatrix} \tag{12}$$

yields the two-dimensional modal sensor equation, whose form is identical to Eq. (5) except the entries of $[B]$ are given by

$$B_{rs} = -\bar{z}_r \int_0^a \int_0^b F_r(x,y)P_{0,r}(x,y)L_p[w_s(x,y)]\,\mathrm{d}y\,\mathrm{d}x \tag{13}$$

Here the indices lm in Eq. (11) depend on the position s defined by the arrangement in Eq. (12). We examined a simply supported rectangular plate, whose normalized modes and frequencies are given by

$$w_s(x,y) = \frac{2}{\sqrt{\rho hab}}\sin\frac{l_s\pi x}{a}\sin\frac{m_s\pi y}{b}, \qquad (s = 1,2,\ldots)$$

$$\omega_s = \pi^2\left[\left(\frac{l_s}{a}\right)^2 + \left(\frac{m_s}{b}\right)^2\right]\sqrt{\frac{D_E}{\rho h}}$$

where ρh is the effective mass/area of the laminate.

One possible choice for the spatial electrode pattern is[5]

$$F_r(x,y)P_{0,r}(x,y) = \mu_r \sin(i_r\pi x/a)\sin(j_r\pi y/b) \tag{14}$$

where the indices ij correspond to r just as lm does to s. For a simply supported plate, putting Eq. (14) into Eq. (13) yields

$$B_{rs} = \frac{2\pi^2\mu_r\bar{z}_r}{\sqrt{\rho hab}}\left(e^0_{31,r}i_r^2\frac{b}{a} + e^0_{32,r}j_r^2\frac{a}{b}\right)\delta_{rs} \tag{15}$$

which is, indeed, a modal sensor based on linear plate vibration theory. For this approach, not only do the lamina have to be cut, but to sense more than one mode, they must be stacked, which can increase the mass and stiffness properties of the structure and, hence, may alter the mode shapes upon which their design was based.

Analogous to the one-dimensional case, we investigated rectangular segmented strips of the form

$$F_r(x,y)P_{0,r}(x,y) = [H(x - x_r) - H(x - x_r - a_r)]$$

$$\times [H(y - y_r) - H(y - y_r - b_r)] \tag{16}$$

In the y direction, the rth the strip begins at y_r with b_r, x_r, and a_r defined earlier. Substituting Eq. (16) into Eq. (13) for a simply supported plate yields

$$B_{rs} = \frac{2\bar{z}_r}{\sqrt{\rho hab}}\left\{\left[e^0_{31,r}\left(\frac{l_s b}{m_s a}\right) + e^0_{32,r}\left(\frac{m_s a}{l_s b}\right)\right]\cos\frac{l_s\pi x}{a}\Bigg|_{x_r}^{x_r+a_r} \times \cos\frac{m_s\pi y}{b}\Bigg|_{y_r}^{y_r+b_r} - 2e^0_{36,r}\sin\frac{l_s\pi x}{a}\Bigg|_{x_r}^{x_r+a_r}\sin\frac{m_s\pi y}{b}\Bigg|_{y_r}^{y_r+a_r}\right\} \tag{17}$$

As in the beam case, $[B]$ is fully populated. For bending sensors, it is common to set $e^0_{36} = 0$, since for commercially available films, e^0_{36} is introduced through a coordinate transformation[12] of the plate axes. Since we want to sense only bending modes, we will do the same. To facilitate the analysis, we set $e^0_{31,r} = e^0_{32,r}$, which yields

$$B_{rs} = \frac{2\bar{z}_r e^0_{31,r}}{\sqrt{\rho hab}}\left[\frac{l_s b}{m_s a} + \frac{m_s a}{l_s b}\right]\cos\frac{l_s\pi x}{a}\Bigg|_{x_r}^{x_r+a_r}\cos\frac{m_s\pi y}{b}\Bigg|_{y_r}^{y_r+b_r} \tag{18}$$

Two-Dimensional Case II: Circular Composite Plate

A circular plate clamped at its outer radius is another case where the natural modes are orthogonal. Here, the partial derivatives of w are transformed into polar coordinates using the chain rule.[13] For a circular composite plate with piezoelectric laminae, given the material constants e^0_{31}, e^0_{32}, and e^0_{36}, the output charge is given in polar coordinates by (note that r is a variable for the circular plate analysis, not an index)

$$q_k(t) = -\bar{z}_k \int_0^{2\pi}\int_0^a F_k P_{0,k}\left\{\left(e^0_{31}\cos^2\theta + e^0_{32}\sin^2\theta + e^0_{36}\sin 2\theta\right)\frac{\partial^2 w}{\partial r^2}\right.$$

$$+\left(e^0_{31}\sin^2\theta + e^0_{32}\cos^2\theta - e^0_{36}\sin 2\theta\right)\left(\frac{1}{r}\frac{\partial w}{\partial r} + \frac{1}{r^2}\frac{\partial^2 w}{\partial\theta^2}\right)$$

$$\left.+2\left(\frac{e^0_{32}-e^0_{31}}{2}\sin 2\theta + e^0_{36}\cos 2\theta\right)\frac{\partial}{\partial r}\left(\frac{1}{r}\frac{\partial w}{\partial\theta}\right)\right\}_k r\,\mathrm{d}r\,\mathrm{d}\theta \quad (19)$$

Here, a is the radius of the circular plate. If $e^0_{32} = e^0_{31}$ and $e^0_{36} = 0$, then Eq. (19) simplifies to

$$q_k(t) = -\bar{z}_k e^0_{31,k}\int_0^{2\pi}\int_0^a F_k P_{0,k}\nabla^2 w r\,\mathrm{d}r\,\mathrm{d}\theta \quad (20)$$

where the Laplacian operator is defined in polar coordinates as $\nabla^2 = \partial^2/\partial r^2 + 1/r(\partial/\partial r) + 1/r^2(\partial^2/\partial\theta^2)$. As a test case, we considered a clamped circular plate. A convenient modal expansion for this case has the form[13]

$$w(r,\theta,t) = \sum_{m=1}^{\infty} w_{0m}(r)\eta_{0m}(t)$$

$$+\sum_{l=1}^{\infty}\sum_{m=1}^{\infty}\left[w_{lmc}(r,\theta)\eta_{lmc}(t) + w_{lms}(r,\theta)\eta_{lms}(t)\right] \quad (21)$$

where

$$w_{0m}(r) = \frac{1}{\sqrt{2\pi\rho h a^2}}\left[\frac{J_0(\beta_{0m}r)}{J_0(\beta_{0m}a)} - \frac{I_0(\beta_{0m}r)}{I_0(\beta_{0m}a)}\right]$$

$$\left.\begin{matrix} w_{lmc}(r,\theta) \\ w_{lms}(r,\theta)\end{matrix}\right\} = \frac{1}{\sqrt{\pi\rho h a^2}}\left[\frac{J_l(\beta_{lm}r)}{J_l(\beta_{lm}a)} - \frac{I_l(\beta_{lm}r)}{I_l(\beta_{lm}a)}\right]\left\{\begin{matrix}\cos l\theta \\ \sin l\theta\end{matrix}\right.$$

$$(l, m = 1, 2, \ldots)$$

and J_l and I_l are Bessel and modified Bessel functions of the first kind and order l. Here, the eigenfunctions $w_{0m}(r)$ are the axisymmetric modes with unique frequencies ω_{0m}. For each frequency $\omega_{lm}(l > 0)$, however, there are two degenerate modes. Thus, any pair of modes that satisfies the boundary conditions and are orthogonal to each other will serve as suitable eigenfunctions. It is natural to select the sine $w_{lms}(r,\theta)$ and cosine $w_{lmc}(r,\theta)$ modes as this pair, since sine and cosine functions of the same argument are orthogonal to each other. The quantities $\beta_{lm}a$ satisfy the characteristic equation

$$I_l(\beta_{lm}a)J_{l-1}(\beta_{lm}a) - J_l(\beta_{lm}a)I_{l-1}(\beta_{lm}a) = 0$$

which yields the corresponding natural frequencies

$$\omega_{lm} = (\beta_{lm}a)^2\sqrt{D_E/\rho h a^4}$$

Arranging the modes according to

$$\begin{bmatrix} \eta_1 & \eta_2 & \eta_7 & \cdots \\ \eta_3 & \eta_5 & \eta_{10} & \cdots \\ \eta_4 & \eta_6 & \eta_{11} & \cdots \\ \eta_8 & \eta_{12} & \eta_{14} & \cdots \\ \eta_9 & \eta_{13} & \eta_{15} & \cdots \\ \vdots & \vdots & \vdots & \ddots \end{bmatrix} = \begin{bmatrix} \eta_{01} & \eta_{02} & \eta_{03} & \cdots \\ \eta_{11c} & \eta_{12c} & \eta_{13c} & \cdots \\ \eta_{11s} & \eta_{12s} & \eta_{13s} & \cdots \\ \eta_{21c} & \eta_{22c} & \eta_{23c} & \cdots \\ \eta_{21s} & \eta_{22s} & \eta_{23s} & \cdots \\ \vdots & \vdots & \vdots & \ddots \end{bmatrix} \quad (22)$$

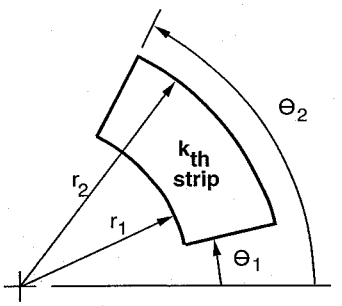

Fig. 3 Segmented strip suitable for the circular plate.

leads to the familiar charge-modal coordinate relation (5), where

$$B_{kj} = -\bar{z}_k e^0_{31,k}\int_0^{2\pi}\int_0^a F_k P_{0,k}\nabla^2 w_j r\,\mathrm{d}r\,\mathrm{d}\theta \quad (23)$$

Here, we consider the upper left $N \times (2N-1)$ portion of the modal coordinate matrix in an attempt to include the modes with the lowest frequencies.

A uniform segmented strip with boundaries suitable for polar coordinates has the form

$$F_k P_{0,k} = \left[H\left(r - r_1^k\right) - H\left(r - r_2^k\right)\right]\left[H\left(\theta - \theta_1^k\right) - H\left(\theta - \theta_2^k\right)\right] \quad (24)$$

Figure 3 shows the dimensions of the strip. For sensors of this type, the entries of $[B]$ can be found explicitly. One must be careful in sensor placement, however, because an ill-conditioned $[B]$ matrix may occur.[14]

For a circular plate, one can also use precut rectangular strips. For this case, the entries of $[B]$ cannot be found in closed form, requiring numerical integration techniques.

III. Extraction of Modal Coordinates

We have formulated the preceding plate analysis so that we can apply the same techniques to both the beam and the plates. Hence, the subsequent analysis will be applicable to all three cases considered. The beam and plate analyses now only differ by the coefficient matrix $[B]$.

The matrix $[B]$ can be partitioned into N (N^2 for the rectangular plate, $N[2N-1]$ for the clamped circular plate) modeled and $n - N(n^2 - N^2, n[2n-1] - N[2N-1])$ residual portions

$$\{q(t)\} = [B_m \quad B_R]\left\{\begin{matrix}\eta_m(t) \\ \eta_R(t)\end{matrix}\right\} \quad (25)$$

Since there are only $N(N^2, N[2N-1])$ strips, only this many measurements can be taken at one time. This is accomplished by inverting $[B_m]$ to obtain modal coordinate measurements (denoted by $\hat{\eta}$)

$$\{\hat{\eta}(t)\} = [B_m]^{-1}\{q(t)\} \quad (26)$$

Substituting Eq. (26) into Eq. (25) yields

$$\{\hat{\eta}(t)\} = \{\eta_m(t)\} + [B_m]^{-1}[B_R]\{\eta_R(t)\} \quad (27)$$

The measured modal coordinate $\hat{\eta}_r(t)$ is the true coordinate plus residual mode contamination.

At this point, one is equipped to compare the order of magnitude of the contamination caused by residual dynamics with other types of sensors. It is shown in Ref. 14 that the asymptotic behavior ($s \to \infty$) of a one-dimensional structure is governed by

$$\omega_s \sim c_s s^h$$

$$w_s(x) \sim d_s\sin(s\pi x) + e_s\cos(s\pi x), \quad (s = 1, 2, \ldots)$$

where $2h$ is the highest order spatial derivative in the equation of motion. For example, for a beam $2h = 4$ and for a string $2h = 2$. Here, c_s, d_s, and e_s are coefficients.

The preceding results for the simply supported beam apply exactly the same way for any type of beam, regardless of boundary

Table 1 Higher mode contamination for different sensor types

Sensor type	Order of contamination
Point displacement sensors (displacement or velocity)	$\mathcal{O}(1)$
Point slope sensors (slope or velocity of slope)	$\mathcal{O}(s)$
Strain gauges	$\mathcal{O}(s^2)$
Full coverage piezoelectric lamina	$\mathcal{O}(s)$
Small coverage piezoelectric lamina	$\mathcal{O}(s^2)$

conditions and mass and stiffness distributions. One may classify the different types of sensors and examine the orders of $[B_m]^{-1}[B_R]$. Note that for this analysis to be valid for the general case, it is assumed that the sensors are relatively evenly distributed and that elements $[B_m]$ and $[B_m]^{-1}$ are of order $\mathcal{O}(1)$. What remains is to analyze the entries of $[B_R]$. Table 1 shows the order of higher mode effects for different sensor types.

For strain gauges, the strain is proportional to the second derivative of deformation for beams. As shown, piezosensors with extremely small surface area perform just like strain gauges. This is to be expected; Eq. (1) indicates that the charge is proportional to the integral of the strain. These orders of magnitude have to be considered together with the amplitudes of the modal coordinates. As discussed in Ref. 9, the higher mode effects in $\{\hat{\eta}(t)\}$ can be made less observable by using piezosensor shapes with better filtering properties. For dynamic analysis, however, it will be shown that measurements obtained from simple rectangular shapes fed through modal state estimators (observers) give satisfactory results. Rather than concern ourselves with the spatial filtering properties of each sensor, we leave this task to the modal state estimators.

In the example for the one-dimensional case, we used equal length sensors and defined a length parameter p, where $0 \leq p \leq 1$. The segmented strips then have the form

$$x_r = \left[r - \tfrac{1}{2}(1+p)\right](a/N), \qquad a_r = p(a/N)$$

For practical modeling purposes, we used the first $n = 10$ modes and tried to sense the first $N = 3$ coordinates. With continuous coverage,

$$[B_m]^{-1}[B_R] = \begin{bmatrix} 0 & 5 & 0 & 7 & 0 & 0 & 0 \\ 2 & 0 & 0 & 0 & 4 & 0 & 5 \\ 0 & 0 & 0 & 0 & 0 & 3 & 0 \end{bmatrix} \tag{28}$$

$$p = 1, \qquad [\mathcal{O}(s)]$$

As coverage vanishes,

$$[B_m]^{-1}[B_R] = \begin{bmatrix} 0 & 25 & 0 & -49 & 0 & 0 & 0 \\ 4 & 0 & 0 & 0 & -16 & 0 & -25 \\ 0 & 0 & 0 & 0 & 0 & -9 & 0 \end{bmatrix}$$

$$p \to 0, \qquad [\mathcal{O}(s^2)]$$

For true point displacement sensors located where coverage goes to zero,

$$[B_m]^{-1}[B_R] = \begin{bmatrix} 0 & 1 & 0 & -1 & 0 & 0 & 0 \\ 1 & 0 & 0 & 0 & -1 & 0 & -1 \\ 0 & 0 & 0 & 0 & 0 & -1 & 0 \end{bmatrix}, \qquad [\mathcal{O}(1)]$$

Thus, as $p \to 0$, the strips act as strain gauges, with residual mode effects proportional to s^2 (as opposed to s for $p = 1$). From this observation, for equal distribution among the strips $p = 1$ leads to the least amount of contamination by higher modes.

It follows from the preceding argument that to minimize residual dynamic effects one is best served by using point displacement sensors. This is so because the measurements are directly related to displacements not to their derivatives (which introduces mode number magnification to the residual modes). This is not possible under many realistic conditions, however, because the displacement sensors need to be attached to a fixed reference frame. As will be shown in the numerical examples, piezosensors with a relatively significant amount of coverage do a good job, especially after their signals are processed by modal observers.

Similar to the beam, we examined rectangular strips for the rectangular plate model, except N^2 modes were measured for symmetry. Using the same coverage parameter p, we then have

$$x_r = \left[l_r - \tfrac{1}{2}(1+p)\right](a/N), \qquad a_r = p(a/N)$$

$$y_r = \left[m_r - \tfrac{1}{2}(1+p)\right](b/N), \qquad b_r = p(b/N)$$

For the simply supported rectangular plate model, we used $N^2 = 3 \times 3 = 9$ sensors with an $n^2 = 100$ mode simulation. For the clamped circular plate, we set $N = 2$ and $n = 10$, giving us 6 sensors on a 190 mode model. $[B_m]^{-1}[B_R]$ is a 9×91 matrix for the rectangular plate and a 6×184 matrix for the circular plate, so we will not include them here, but the same principles apply, since the asymptotic behavior of the eigensolution of plates is similar to that of a beam. The higher mode participation effects are more pronounced for the plates since the eigenvalues are more closely spaced than they are for beam problems. This is especially true for the lower modes, which is the concern of this paper.

IV. Modal Observers

Using charge measurements, we have extracted a modal coordinate measurement, but we still need a modal velocity. One can take the time derivative of Eq. (27) to obtain modal velocity estimates, but using modal observers has been proven to be more reliable.[15] The modal coordinates satisfy the uncoupled equations

$$\dot{\boldsymbol{x}}_r(t) = \begin{bmatrix} 0 & 1 \\ -\omega_r^2 & 0 \end{bmatrix} \boldsymbol{x}_r(t) + \begin{bmatrix} 0 \\ 1 \end{bmatrix} \mathcal{N}_r(t)$$

$$y_r(t) = \begin{bmatrix} 1 & 0 \end{bmatrix} \boldsymbol{x}_r(t) \tag{29}$$

where

$$\boldsymbol{x}_r(t) = [\eta_r(t) \quad \dot{\eta}_r(t)]^T, \qquad y_r(t) = \eta_r(t)$$

and $\mathcal{N}_r(t)$ is the modal forcing for the rth mode. A full-order state estimator (observer) for Eq. (29) has the form[16]

$$\dot{\boldsymbol{z}}_r(t) = \begin{bmatrix} -k_{r,1} & 1 \\ -\omega_r^2 - k_{r,2} & 0 \end{bmatrix} \boldsymbol{z}_r(t) + \begin{bmatrix} k_{r,1} \\ k_{r,2} \end{bmatrix} \eta_r(t) + \begin{bmatrix} 0 \\ 1 \end{bmatrix} \mathcal{N}_r(t)$$

where

$$\boldsymbol{z}_r(t) = [\hat{\eta}_r(t) \quad \dot{\hat{\eta}}_r(t)]^T$$

are the estimates for $\boldsymbol{x}_r(t)$. Closed-form expressions can be found for the gain matrix $\boldsymbol{K}$

$$\begin{bmatrix} k_{r,1} \\ k_{r,2} \end{bmatrix} = \begin{bmatrix} -(\lambda_1 + \lambda_2) \\ \lambda_1\lambda_2 - \omega_r^2 \end{bmatrix} \tag{30}$$

If the entries of $\boldsymbol{K}$ are chosen such that eigenvalues λ_1 and λ_2 of the observer have negative real parts, then $\boldsymbol{z}(t) - \boldsymbol{x}(t) \to 0$ as $t \to \infty$. Since the true modal coordinates are not known, the measurements $\hat{\eta}_r(t)$ are used to drive the modal observers. This is different than traditional Luenberger observers, in which one or more of the state variables is also the output. Here, the modal coordinate measurements are fed through the modal observers to estimate themselves, as well as modal velocities. The modal observer acts to filter out residual dynamics and smooth out noise contamination, as well as give a velocity estimate.

Also note the observer defined above is for charge measurements. If the current is measured, a modal velocity measurement can be obtained, since electric current is the time derivative of charge. In this case, the form of the observers and gain matrix entries must be modified, but the approach is the same.

V. System Errors and Disturbances

We next analyze the effects that need to be considered in an actual real-time observation. All of these effects couple the modal observer equations with each other and should result in deterioration of the performance of the modal observers.

Noise Effects

In an attempt to model noise, we assume that the charge is affected by some small quantity

$$\hat{q}_r(t) = q_r(t) + \epsilon_r, \qquad \epsilon_r = \Delta_r q_r(t) \tag{31}$$

in which Δ_r is a uniform random number. Using the preceding approach, we obtain for the measurements

$$\{\hat{\eta}(t)\} = \{\eta_m(t)\} + [B_m]^{-1}[\Delta][B_m]\{\eta_m(t)\} + [B_m]^{-1}[I + \Delta][B_R]\{\eta_R(t)\} \tag{32}$$

where $[\Delta]$ is a diagonal matrix with random elements. We see that noise modeled in this fashion further corrupts the modal coordinate measurements by coupling the observed modes.

Note that if the properties of the noise are known and the noise amplitudes are large, one can use modal Kalman filters to estimate the modal coordinates and velocities.[17,18] Our objective in including noise in the system simulations here is to examine the degradation in the observer performance due to noise that is not accounted for. As we shall demonstrate later in this paper, moderate amounts of noise have virtually no effect on the observer performance, making it unnecessary to use modal Kalman filters, at least for the examples considered.

Damping Effects

In all real physical systems, there is some damping present. Not including a modal damping term or including an incorrect damping term in the observer equations makes the model unrealistic, but the modal observers inherently account for this by choice of the observer gains. In the presence of damping, the modal equations become

$$\dot{x}_r(t) = \begin{bmatrix} 0 & 1 \\ -\omega_r^2 & -2\zeta_r\omega_r \end{bmatrix} x_r(t) + \begin{bmatrix} 0 \\ 1 \end{bmatrix} u_r(t)$$

$$y_r(t) = [1 \quad 0] x_r(t)$$

For a desired set of eigenvalues λ_1 and λ_2, the gain matrix becomes

$$\begin{bmatrix} k_{r,1} \\ k_{r,2} \end{bmatrix} = \begin{bmatrix} -(\lambda_1 + \lambda_2 + 2\zeta_r\omega_r) \\ \lambda_1\lambda_2 - \omega_r^2 + 2\zeta_r\omega_r(\lambda_1 + \lambda_2 + 2\zeta_r\omega_r) \end{bmatrix}$$

In comparison to Eq. (30), by including damping in the observer model, we require less gain for the same pole placement.

Discretization Effects

For very simple plate and beam geometries, exact solutions of the eigenvalue problem exist. In general, however, complicated geometries and boundary conditions do not permit such results. To analyze the effects of spatial discretization, we use the assumed modes method.[13] For this approach we choose a finite series of n twice-differentiable linearly independent admissible functions $\psi_j(x)$ which satisfy the geometric boundary conditions without overconstraining the problem. The mode shape approximations $\phi_i(x)$ are then related to these functions by

$$\phi_i(x) = \sum_{j=1}^{n} U_{ji}\psi_j(x) \tag{33}$$

where the columns of the matrix U_{ij} are the normalized eigenvectors of the discrete eigenvalue problem resulting from the application of the assumed modes method. For the beam case, we used the following set of linearly independent polynomials:

$$\psi_j\left(\frac{x}{a}\right) = \frac{x}{a}\prod_{i=1}^{j}\left(1 - \frac{j}{i}\frac{x}{a}\right) \tag{34}$$

The natural frequencies of the discretized system (for order of discretization $n = 5$) are

$$\{\tilde{\omega}\} = \{9.870, 39.65, 90.34, 276.0, 508.4\}\sqrt{D_E/\rho hba^4}$$

From the exact solution to the eigenvalue problem,

$$\{\omega\} = \{9.870, 39.48, 88.83, 157.9, 246.7\}\sqrt{D_E/\rho hba^4}$$

we see that five admissible functions give good approximations to the first three eigenvalues.

Discretization can also be done for the simply supported plate model, except some care must be used when integrating the biharmonic stiffness operator by parts. For the rectangular plate, our set of trial functions has a similar form,

$$\psi_{rs}(x, y) = \frac{x}{a}\frac{y}{b}\prod_{i=1}^{r}\left(1 - \frac{r}{i}\frac{x}{a}\right)\prod_{j=1}^{s}\left(1 - \frac{s}{j}\frac{y}{b}\right) \tag{35}$$

One must use caution when numerically computing the discrete eigenvectors. Depending on method of solution, they may not be properly normalized, and the order of magnitude of the natural frequencies may not coincide with the index arrangement defined earlier.

Continuing with the beam, now denote $[\tilde{B}]$ as the charge/modal coordinate matrix using the trial functions. Thus, Eq. (32) becomes

$$\{\tilde{\eta}(t)\} = [\tilde{B}_m]^{-1}[I + \Delta][B_m]\{\eta_m(t)\} + [\tilde{B}_m]^{-1}[I + \Delta][B_R]\{\tilde{\eta}_R(t)\} \tag{36}$$

with

$$\tilde{B}_{rs} = -e^0_{31,r}\bar{z}_r\mu_r\left[\left.\frac{d\phi_s(x)}{dx}\right|_{x_r+a_r} - \left.\frac{d\phi_s(x)}{dx}\right|_{x_r}\right]$$

For the plate discretization, the computed eigenvectors must be arranged according to the preceding index assignment (12) or (22) before computing $[\tilde{B}_m]$.

VI. Observer Performance

Beam Results

We will first show the reconstructed modal velocities and coordinates for the beam, using a three strip model with full coverage subject to the following loading and initial conditions:

$$q(x, t) = 20\sin(3\pi^2 t)(x/a)[1 - (x/a)^2]$$

$$w_0(x) = (x/a)[1 - (x/a)], \qquad \dot{w}_0(x) = x/a$$

We used the approximate mode shapes derived earlier and included uniform measurement noise with $\Delta = [-0.05, 0.05]$. Thus, the natural frequencies that used in the observers were those computed from the discretization analysis. We included system damping $\zeta_r = 0.01$ in the solution but modeled no observer damping to illustrate that errors in damping properties are not critical. After experimenting with several different observer pole configurations, we found that complex conjugate poles of the form

$$\left.\begin{matrix}\lambda_1 \\ \lambda_2\end{matrix}\right\}_r = Re \pm j\tilde{\omega}_r \tag{37}$$

gave the best results. This is not as evident in the beam analysis as it was in the plate response. The imaginary part of the pair gives the oscillating frequency of the observer response, so we set it equal to the corresponding natural frequency. This is why we need accurate estimates for ω_r. Figure 4a gives the third true modal velocity plotted with its corresponding observer for $Re = -5$.

We next checked the observer quantities corresponding to the modal displacements. Referring to Fig. 4b, we see that for the second modal coordinate, the observer was closer to the true value than the measurement itself. We also ran cases where beam loading was present but not modeled in the observer. The results indicated that the observers work very well even in the presence of known as well as unknown external excitation.[14] Also note that for the third

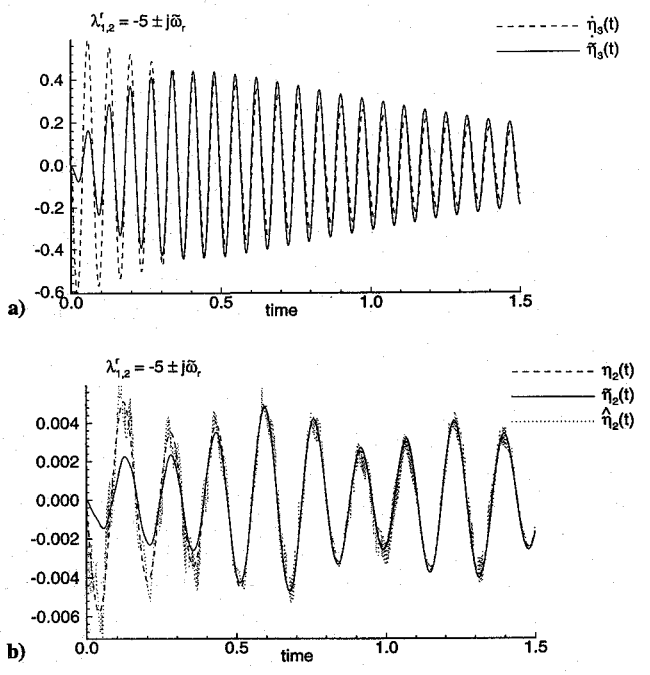

Fig. 4 Modal observer estimates for the beam for a) $\dot{\eta}_3$ and b) η_2.

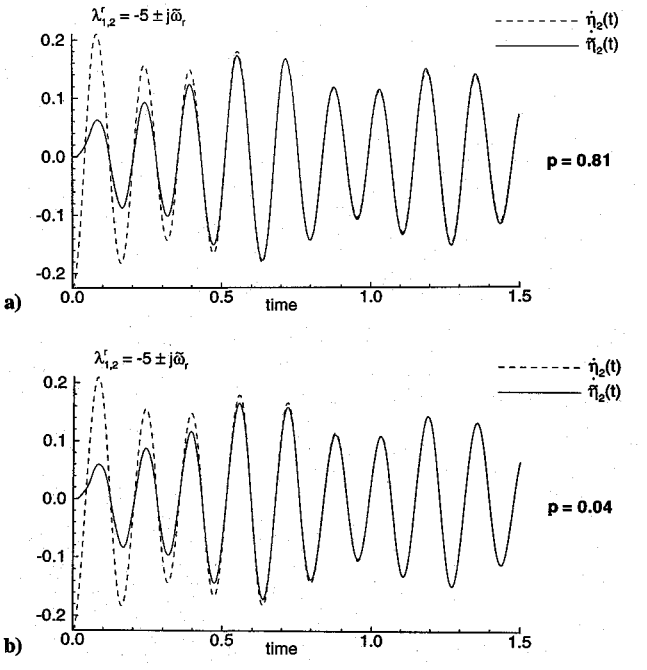

Fig. 5 Modal observer estimate for $\dot{\eta}_2$ with a) $p = 0.81$ and b) $p = 0.04$.

mode (Fig. 4a), there is a lag between the true modal velocity and its observer estimate. The modal observers are constantly trying to keep up with the system motion.

We next reduce the lengths of the strips by decreasing the coverage parameter p. For the beam, the coverage area is linearly proportional to p. The results for the second modal velocity $\dot{\eta}_2(t)$ are shown in Fig. 5. For this set of plots, we used the same parameters as before except we set $\zeta_r = 0$. The modal velocity extraction deteriorates very little as the coverage becomes smaller. A smaller pattern was observed for the modal displacements. It should be noted that all of the simulations described were also conducted for cases where each piezosensor was of different length or the distribution of the sensors on the beam was not even. There was no discernable difference in the results.

Next, we introduce parameter uncertainties to the modal coordinate extraction process. These deteriorate the extraction results by making the $[\tilde{B}_m]$ matrix even more different from $[B_m]$. As an

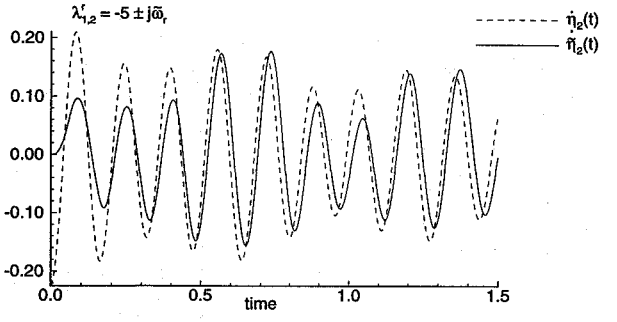

Fig. 6 Modal observer response for $\dot{\eta}_2$ with a point mass error.

illustration, consider a point mass per unit width added to the beam, modeled as $M = 0.1\rho hab$ at $x/a = 0.25$. This gives the first three natural frequencies $\{\tilde{\omega}\} = \{9.405, 36.45, 87.56\}\sqrt{D_E/\rho hba^4}$. We treat the point mass as a mass distribution error by including it in the discretization calculation of $[\tilde{B}_m]$ but not in the true system dynamics. The observer response for the second modal velocity with $\Delta = 0.05$ is shown in Fig. 6. System damping was omitted for clarity. Although the amplitude is smaller than the true value, the modal observer gives accurate frequency response with a constant phase lag. The modal observers converge to the proper frequency, even with a significant error in the mass distribution.

In all of the beam calculations, $B_{r6} = 0\,(r = 1, 2, 3)$. For the sixth mode of a simply supported beam, $w_6(x) \sim \sin(6\pi x/a)$, so that

$$w_6'(0) = w_6'\left(\frac{a}{3}\right) = w_6'\left(\frac{2a}{3}\right) = w_6'(a)$$

Thus, for $N = 3$ strips and full coverage,

$$B_{r6} = -\mu_r \bar{z}_r e^0_{31,r}\left[w_6'\left(r\frac{a}{3}\right) - w_6'\left((r-1)\frac{a}{3}\right)\right] = 0$$

So our strip layout for the beam is incapable of sensing the sixth mode. For the simply supported beam, full coverage with N equal length strips automatically filters out the $2N$th mode. A similar behavior was seen in the simply supported plate model. This sensor output cancellation was also observed by Tzou and Fu.[7] Since the strip edges lie on two similar nodal lines, the charges generated within the sensor effectively cancel out. If any one of the N sensors is used to measure a mode it cannot detect, this leads to an ill-conditioned $[B_m]$ matrix.[14] This makes it difficult to obtain a modal coordinate estimate, since $[B_m]$ must be invertible according to Eq. (26). In this case modal coordinate extraction becomes even more difficult when measurement noise is introduced.

Rectangular Plate Results

First, we simulated a simply supported rectangular plate with $b = 1.5a$ and full 3×3 sensor coverge subject to an impulse loading

$$\hat{F}_0 = 1, \qquad \text{at} \qquad x/a = 0.4, \qquad y/b = 0.7$$

Measurement noise with $\Delta = [-0.05, 0.05]$ was also included; approximate mode shapes and observer frequencies were found using a 5×5 discretization with the two-dimensional trial functions given by Eq. (35). Figure 7 shows some modal observer results with $Re = -8$.

For the higher modes, we found that the amplitudes of both of the reconstructed coordinates and velocities were smaller than the true modal values. The frequencies for these modes were simply too fast for the observers to keep up. This can be remedied by making the real part of the modal observer poles more negative, speeding up the convergence rate but also increasing sensitivity to sources of error. All modal observers showed excellent agreement with the true vibration frequencies.

To compare coverage effects to the beam, we note that for the rectangular plate the sensor coverage area is proportional to p^2. Thus, to make a fair comparison between the simply supported beam and rectangular plate models, the values we select for p for the plate

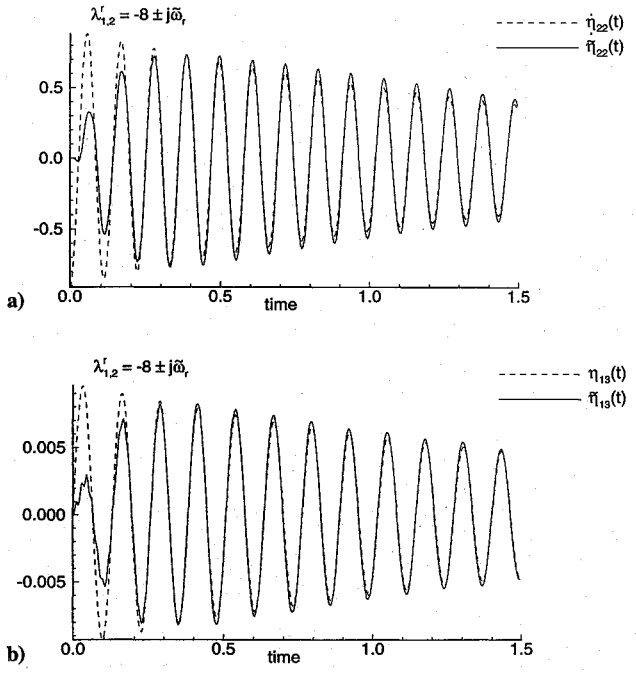

Fig. 7 Observer estimates for the rectangular plate for a) $\dot{\eta}_{22}$ and b) η_{13}.

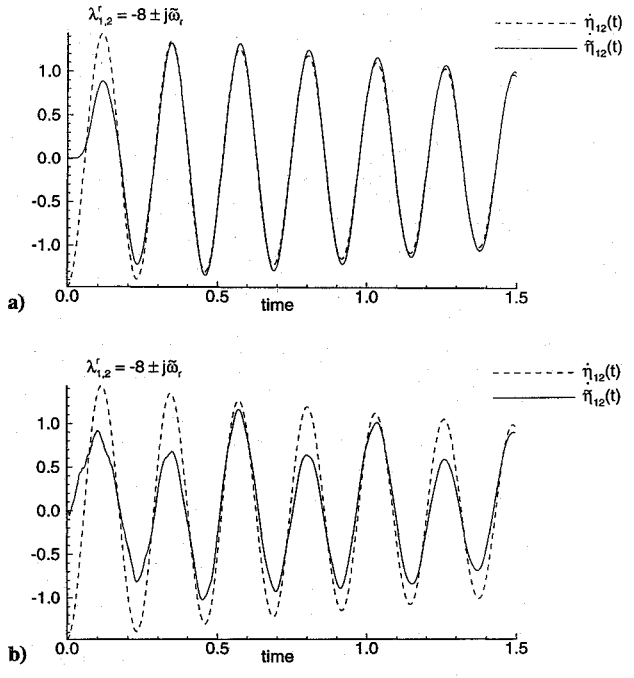

Fig. 8 Effect of coverage on $\dot{\eta}_{12}$ for a) $p = 0.9$ and b) $p = 0.2$.

must be the square root of the values used in Fig. 5. Figure 8 shows the effect of decreasing coverage on the extraction of $\dot{\eta}_{12}(t)$ using the appropriate values of p. The modal observers for the rectangular plate are much more sensitive to p than those for the beam, given the same relative coverage area. As mentioned earlier, this is due to smaller spacing between the plate natural frequencies.

Circular Plate Results

Next, we simulated a clamped circular plate with the strip layout shown in Fig. 9 subject to an impulse loading

$$\hat{F}_0 = 100, \qquad \text{at} \qquad r/a = 0.2, \qquad \theta = \pi/6$$

We also included noise with $\Delta = [-0.05, 0.05]$ and the first 190 modes based on the modal coordinate index arrangement defined for

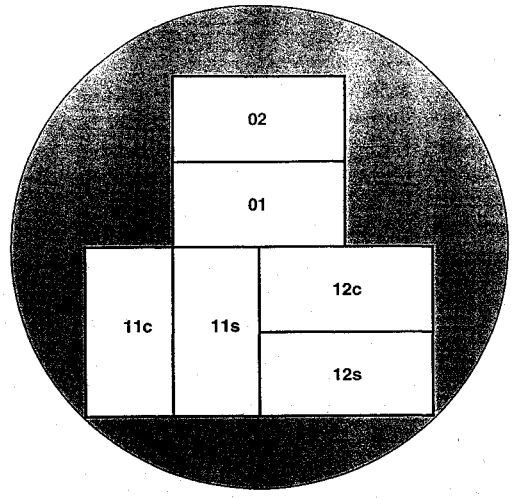

Fig. 9 Strip layout for clamped circular plate model.

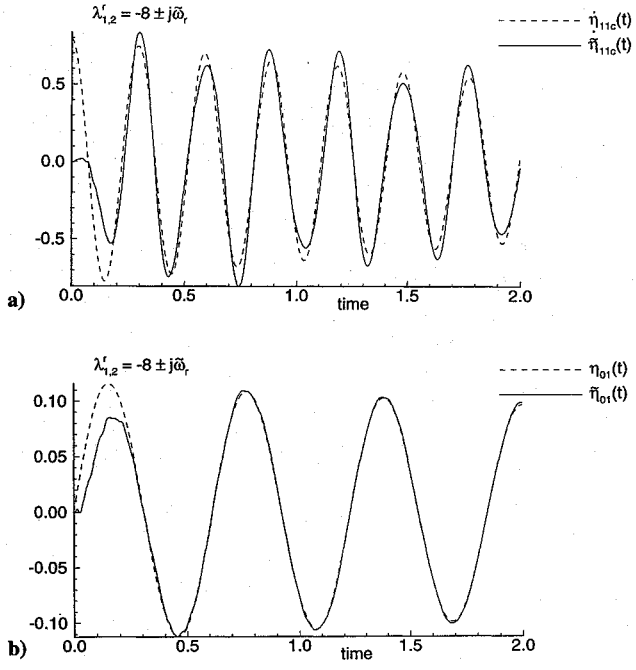

Fig. 10 Observer estimates for the circular plate for a) $\dot{\eta}_{11c}$ and b) η_{01}.

the circular clamped plate. The modal observer poles were chosen with $Re = -8$. Here, system damping with $\zeta_r = 0.01$ was included but discretization effects were omitted. Figure 10 shows some modal observer results for the circular plate model.

Not only are the circular plate frequencies more closely spaced than those for the rectangular plate, they are degenerate for all modes higher than the axisymmetric modes (w_{lmc} and w_{lms} have the same vibration frequency ω_{lm}). This is the main reason for the chatter of the $\eta_{01}(t)$ observer about its true modal coordinate in Fig. 10b.

Although the modal observers for the circular plate never converge absolutely for our selected strip layout, they show very good frequency behavior, despite the presence of repeated eigenvalues.

From preceding discussion, we have selected $e^0_{36} = 0$ for all laminae in the plate results. We initially included a nonzero value in the simulation, but we found that it caused substantial steady-state error in the higher mode observers. This material constant is generally introduced for torsion sensors,[12] which may confuse the modal observer in the filtering process as to which bending frequency to converge upon. Regardless, since it may be set to zero in the manufacturing process, we have done so in both the rectangular and circular plate models.

VII. Conclusions

We have presented a method to sense structural vibration by combining modern piezoelectric film technology and modal analysis. In comparison to previously developed orthogonal sensors, using segmented piezoelectric strips sacrifices the ability to directly detect individual modes but eliminates the need for complicated sensor geometries. Satisfactory modal information is obtained once the sensor measurements are processed through modal observers. One can accommodate mass and stiffness variations in the system simply by recalculating the charge/modal coordinate matrices (by spatial discretization, finite element method, etc.) and updating natural frequency approximations in the modal observers. Feeding the measurements through modal observers gives very good results, even with noise, discretization, and modeling errors present.

The results obtained in the one- and two-dimensional analyses indicate the piezoelements are very promising for the measurement of the vibration of elastic bodies. They are lighter in weight, less expensive, and more versatile than traditional discrete sensors. The shape and location of each piezosensor affects the quality of the sensor measurements $\hat{\eta}_r(t)$ due to sensor output cancellation and frequency rolloff behavior. For the method presented here, even simple rectangular shapes yield satisfactory results, once their output is processed through modal observers. The size of the individual elements and the percent area of the structure covered by the piezofilms also cease to be critical issues when the modal observers are used, as long as about one-quarter of the structure is covered. In conclusion, piezoelements as sensors for modal analysis present themselves as viable alternatives to existing measurement approaches.

Acknowledgments

This research was supported by the Federal Aviation Administration. The authors would like to thank Peter Shyprykevich, Technical Monitor, for his helpful comments and suggestions.

References

[1]Collins, S. A., Padilla, C. E., Notestine, R. J., von Flotow, A. H., Schmitz, E., and Ramey, M., "Design, Manufacture, and Application to Space Robotics of Distributed Piezoelectric Sensors," *Journal of Guidance, Control, and Dynamics*, Vol. 15, No. 2, 1992, pp. 396–403.

[2]Crawley, E. F., and de Luis, J., "Experimental Verification of Distributed Piezoelectric Actuators for Use in Precision Space Structures," *Proceedings of the 27th AIAA Structure Dynamics Conference*, AIAA, New York, 1986, pp. 116–124.

[3]Hubbard, J. E., Jr., "Distributed Transducers for Smart Structural Components," *Proceedings of the 6th International IMACS Conf.*, Orlando, FL, 1988.

[4]Kepler, R. G., and Anderson, R. A., "Ferroelectric Polymers," *Advances in Physics*, Vol. 41, No. 1, 1992, pp. 1–57.

[5]Lee, C.-K. and Moon, F. C., "Modal Sensors/Actuators," *Journal of Applied Mechanics*, Vol. 57, June 1990, pp. 434–441.

[6]Tzou, H.-S., "Lightweight Transducer Development using Piezoelectric Polymers," *Proceedings of the 6th International IMACS Conf.*, Orlando, FL, 1988.

[7]Tzou, H.-S., and Fu, H. Q., "A Study on Segmentation of Distributed Piezoelectric Sensors and Actuators: Part 1—Theoretical Analysis," *Journal of Sound and Vibration*, Vol. 172, No. 2, 1994, pp. 247–260.

[8]Tzou, H.-S., and Fu, H. Q., "A Study on Segmentation of Distributed Piezoelectric Sensors and Actuators: Part 2—Parametric Study and Active Vibration Controls," *Journal of Sound and Vibration*, Vol. 172, No. 2, 1994, pp. 261–276.

[9]Andersson, M. S., and Crawley, E. F., "Discrete Shaped Strain Sensors for Intelligent Structures," *Proceedings of the AIAA/ASME/ASCE/AHS 33rd Structures, Structural Dynamics and Materials Conference*, AIAA, Washington, DC, 1992, pp. 566–576.

[10]Baruh, H., and Choe, K., "Sensor Placement in Structural Control," *Journal of Guidance, Control, and Dynamics*, Vol. 13, No. 3, 1990, pp. 524–533.

[11]Meirovitch, L., and Baruh, H., "Implementation of Modal Filters for Control of Structures," *Journal of Guidance, Control, and Dynamics*, Vol. 8, No. 6, 1985, pp. 707–716.

[12]Lee, C. K., "Theory of Laminated Piezoelectric Plates for the Design of Distributed Sensors/Actuators. Part I: Governing Equations and Reciprocal Relationships," *Journal of the Acoustical Society of America*, Vol. 87, No. 3, 1990, pp. 1144–1158.

[13]Timoshenko, S., *Theory of Plates and Shells*, McGraw–Hill, New York, 1959, pp. 257–260.

[14]Callahan, J., "Modal Analysis and Control of Flexible Bodies Using Segmented Piezoelectric Components," Master's Thesis, Dept. of Mechanical and Aerospace Engineering, Rutgers Univ., Piscataway, NJ, Jan. 1995.

[15]Meirovitch, L., *Analytical Methods in Vibrations*, Macmillan, New York, 1967, pp. 179–189, 233–235.

[16]Tadikonda, S. S. K., and Baruh, H., "Gibbs Phenomenon in Structural Mechanics," *AIAA Journal*, Vol. 29, No. 9, 1991, pp. 1488–1497.

[17]Choe, K., and Baruh, H., "Sensor Failure Detection in Flexible Structures Using Modal Observers," *Journal of Dynamic Systems, Measurement and Control*, Vol. 115, No. 3, 1993, pp. 411–418.

[18]Chen, C.-T., *Linear System Theory and Design*, Holt, Rinehart and Winston, Inc., New York, 1984, pp. 354–358.

[19]Kwakernaak, H., and Sivan, R., *Linear Optimal Control Systems*, Wiley, New York, 1972, pp. 339–360.

[20]Oz, H., and Meirovitch, L., "Stochastic Independent Modal Space Control of Distributed Parameter Systems," *Journal of Optimization Theory and Applications*, Vol. 40, No. 1, 1983, pp. 121–154.